

TABLE OF CONTENTS

CHAPTER 1: INTRODUCTION	1
CHAPTER 2: SITE, INSTRUMENTATION, DATA, AND METHODOLOGY	5
2.1 Haukeliseter Site	5
2.2 Climate at Haukeliseter	6
2.3 Instruments	7
2.3.1 Double Fence Snow Gauge	9
2.3.2 MRR - Micro Rain Radar	10
2.3.3 PIP - Precipitation Imaging Package	12
2.3.4 MASC - Multi-Angular Snowfall Camera	12
2.4 Optimal Estimation Retrieval Algorithm	13
2.4.1 Snowfall Retrieval Scheme	14
2.4.2 Environmental Masks for the Optimal Estimation Retrieval	18
2.5 Operational Weather Forecast Model	19
2.5.1 MetCoOP Ensemble Prediction System - MEPS	19
2.5.2 Meso-NH and the ICE3 Scheme	20
2.5.3 Adjustment of ICE3 Inside AROME-MetCoOp	23
2.6 Computing Snowfall Quantities	23
2.6.1 Layer Thickness in MEPS	23
2.6.2 Snow Water Content	24
2.6.3 Snow Water Path	24
2.7 Statistical Methods for Analysing Data	24
2.7.1 Ensemble Mean and Coefficient of Variation	25
2.7.2 Mean Error and Mean Absolute Error	25
2.7.3 Percent Difference and Average Difference	25
CHAPTER 3: ANALYSIS OF THE CHRISTMAS STORM 2016	26
3.1 Extreme Weather	27
3.2 Dynamic Tropopause Map	28
3.3 Thickness, Sea Level Pressure, Total Precipitable Water, and Wind at 250 hPa	28
3.4 Integrated Vapour Transport	31
3.5 Observations at the Weather Mast	33
3.6 Large Scale Circulation	34
CHAPTER 4: SNOW OBSERVATIONS AND MEPS FORECASTS FOR HAUKELISETER	41
4.1 The Christmas Storm 2016	41
4.1.1 Meteorology Comparison	41

4.2	Snowfall	57
4.2.1	Sensitivity of the Optimal Estimation Retrieval	58
4.2.2	Comparison of Surface Observations	60
4.2.3	Comparison of Surface Observations and MEPS	62
4.2.4	Comparison of Snow Water Content in the Vertical	71
4.2.5	Discussion	84
CHAPTER 5: SUMMARY AND OUTLOOK		88
5.1	Outlook	90
LIST OF ABBREVIATIONS		92
REFERENCES		95
APPENDIX A: FORWARD MODEL		103
A.1	Scattering Model	103
APPENDIX B: FORECASTED SNOW WATER CONTENT		105
B.1	Hourly Averages Ensemble Member Zero and One	105
B.2	Vertical Snow Water Content - All Ensemble Members	108

CHAPTER 3: ANALYSIS OF THE CHRISTMAS STORM 2016

Extreme storm Urd was chosen for an in depth examination for a number of intriguing reasons:

- I) the Haukerlister site is a WMO sanctioned weather station with single and double fence rain gauge measurements,
- II) additional instruments were placed at the site for the winter 2016/2017 season allowing for the vertical profiling of snow properties and snowfall accumulation
- III) the MEPS forecasting system had recently become the operational model platform for Met-Norway, and
- IV) the unique temporal evolution of the precipitation properties during the event

A preliminary analysis identified periods of both good agreement of snow accumulation measurements by MEPS in comparison to the ground observations, as well as periods of overestimation by MEPS. The above factors make for an interesting study to assess and better understand the usefulness of the measurements in question.

The next sections will provide a definition of an extreme weather event, a description of the weather maps that were utilized, and a presentation of the synoptic scale evolution of the storm.

Prior to the analysis, each weather maps' purpose will be presented to understand the connections between them. All the weather maps are generated using data from ECMWF operational model Cycle 43r1. The analysis consists of 137 model levels and to reduce computational costs it is reduced to the *octahedral reduced Gaussian grid* and then interpolated to a N640 Gaussian grid. Between the pole and the equator are 640 lines of latitude equally symmetric spaced. This follows 1280 latitude lines for each hemisphere. The resolution along the longitude is $90^\circ/640$ lines with points getting closer with increasing latitude. This follows a total number of grid points of $8 \cdot 640^2$ [Dando, 2016].

3.1 EXTREME WEATHER

'Extreme weather' is a meteorological term, associated with the extent of a weather type. The Norwegian Meteorological Institute declares an extreme event, if strong winds, large amounts of precipitation and large temperature changes are expected before the event occurs. As well as a large avalanche risk is present and coastal areas are influenced by extremely high-water levels. Generally, an event is divided into four phases by Met-Norway to be called extreme event [Pedersen and Rommetveit, 2013].

Phase A: *Increased monitoring before the possible extreme weather.* The meteorologists give special attention to the weather situation. At this point it is not certain, that there will be an extreme weather event.

Phase B: *Short-term forecasts.* It is decided, that there will be an extreme event. The forecasts are more detailed, and updates will be published at least every six hours. The event will get a name.

Phase C: *The extreme weather is in progress.* The meteorologists send out weather announcements at least every six hours.

Phase D: *The extreme weather event is over. Clean-up and repairs are in progress.* When the extreme weather is over the public is notified and information about the upcoming weather and clearing work is given.

The Christmas storm was considered an extreme event by the Met-Norway, named 'Urd' [Olsen and Granerød, 2017]. The average wind along the coast of Western Norway reached hurricane strength (observed: 40 ms^{-1} to 55 ms^{-1}). In South and Eastern Norway, west to north-west winds between 25 ms^{-1} to 40 ms^{-1} were measured. At Haukeliseter, 136.4 mm of precipitation were measured from 21 to 27 December 2016. The 2016 Christmas storm was just above the limit of been called an extreme weather event.

To understand which damage a storm can have, Færaas et al. [2016] released a table to associate wind strength with damage (see Table 3.1.1).

Table 3.1.1: Damage related to wind speed, from Færaas et al. [2016].

slight storm	20.8 ms^{-1} – 24.4 ms^{-1}	Large trees sway and hiver. Roofs can blow down.
full storm	24.5 ms^{-1} – 28.4 ms^{-1}	Trees are pulled up with clutter. Big damages to houses.
strong storm	28.5 ms^{-1} – 32.6 ms^{-1}	Extensive damage.
hurricane	$>32.6 \text{ ms}^{-1}$	Unusually large destruction.

3.2 DYNAMIC TROPOPAUSE MAP

The dynamic tropopause maps (DT), presented herein (e.g. Figure 3.3.0a) are comprised of the potential temperature (shading) and wind barbs [ms^{-1}] on the two PVU surface (one PV unit = $10^{-6} \text{ m}^2 \text{ s}^{-1} \text{ K kg}^{-1}$), and the 925–850 hPa averaged relative vorticity (black contours - every $0.5 \times 10^{-4} \text{ s}^{-1}$ only positive values are plotted). An example is presented in Figure 3.3.0a. High (low) values of potential temperature represent an elevated (suppressed) tropopause. Regions with a large horizontal gradient of potential temperature indicate a steeply-sloping tropopause that is associated with an enhanced pressure gradient force and winds. From this, the mid-latitude jet stream can be pointed out. The low-level averaged relative vorticity is plotted to provide a three-dimensional (in the vertical) picture of the atmosphere. It is useful for identifying cyclone centres and attendant frontal boundaries.

The 925 –850 hPa layer-averaged surface relative vorticity is shown in black contours, every $0.5 \times 10^{-4} \text{ s}^{-1}$. It represents the rotation of a fluid.

Along the Rossby-Wave-Guide, troughs and ridges are seen which can be combined with the surface relative vorticity to understand the vertical dynamic interaction in the atmosphere. Wave disturbance travel along the wave guide or regions of strong gradients. At the dynamic tropopause level the Rossby-Wave-Guide is the region of strong potential temperature gradient, shading in Figure 3.3.0a [Nielsen-Gammon, 2001]. In case of a westward tilt between the surface cyclone and an upper level through an intensification of the surface cyclone is more likely to occur.

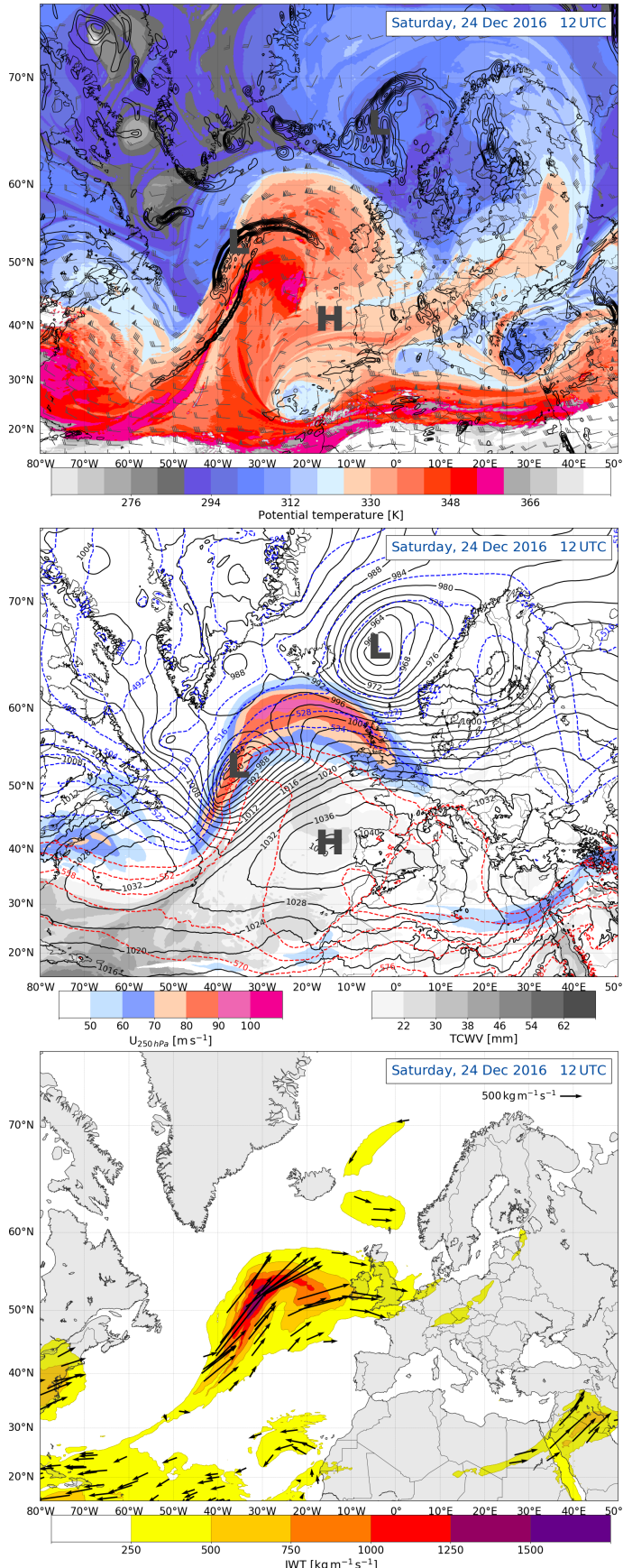
3.3 THICKNESS, SEA LEVEL PRESSURE, TOTAL PRECIPITABLE WATER, AND WIND AT 250 hPa

A complementary view of the three-dimensional structure of the atmosphere is also presented: 250 hPa wind speed (colour shading, m s^{-1}), mean sea level pressure (black contours, hPa), 1000–500 hPa thickness (dashed contours) and the total precipitable water (black-white shading, mm). See Figure 3.3.0b for an example.

The dashed, coloured contours in Figure 3.3.0b show the vertical thickness between the 1000 hPa and 500 hPa surface, every 6 dam. The thickness between two pressure levels can be interpreted via the hypsometric equation (Equation (2.6.3)), which equates the thickness to the mean temperature of the layer in question. In a relative sense, a larger thickness indicates a warmer air mass. In addition, strong horizontal gradients in the thickness field can be related to frontal boundaries. Specific to the discussion in this thesis, the thickness field also provides useful information regarding the form of precipitation (liquid, frozen).

Analysis of the mean sea level pressure can be used to identify cyclones (L) and anticyclones (H) at the surface as well as provide supplementary information regarding frontal boundaries (Figure 3.3.0b). The total precipitable water is a measure of the column integrated moisture. It represents an instantaneous measure of moisture in time and space, which can be useful when assessing the amount of moisture that may fall as precipitation in future time steps. The 250 hPa wind speeds are used to identify strong upper-level flow (i.e. the jet stream) and can be directly

compared to the dynamic tropopause map (Figure 3.3.0a).



a: Dynamic tropopause analysis map at 2 PVU. Potential temperature [K] at the 2 PVU surface, shaded according to the colour bar. Total wind, barbs [m s^{-1}], and 925 – 850 hPa layer-averaged surface relative vorticity (black contours, every $0.5 \times 10^{-4} \text{ s}^{-1}$).

b: Jet, thickness, mean sea level pressure, and total precipitable water synoptic analysis. 250 hPa wind speed, shaded according to the colour bar, [m s^{-1}]. 1000 – 500 hPa thickness, dashed contours every 6 dam, MSLP, black contours every 4 hPa, total column water vapour [mm], shaded according the grey scale.

c: Integrated vapour transport analysis map. Integrated vapour transport, shaded according to the colour bar [$\text{kg m}^{-1} \text{s}^{-1}$]. Vectors, indicating the direction and magnitude of the IVT.

Figure 3.3.1: ECMWF analysis on 24 December 2016 at 12 UTC. L and H indicating the surface low and high pressure, respectively.

3.4 INTEGRATED VAPOUR TRANSPORT

An atmospheric river (AR) is a filament structure of intense moisture transport from the tropics to higher latitudes. Heavy precipitation can be associated with it, because the air is warm and moist. This can often be observed at mountain ranges at west coasts such as in Norway [Azad and Sorteberg, 2017]. Due to orographic lifting the moisture will be released and follow high amounts of precipitation.

An atmospheric river is characterised if the integrated vapour transport shows values higher than $250 \text{ kg m}^{-1} \text{s}^{-1}$ and a continuous region larger than 2000 km [Rutz et al., 2014].

Figure 3.3.0c shows coloured contours of the integrated vapour transport (IVT) in $\text{kg m}^{-1} \text{s}^{-1}$, where warmer colours indicate higher IVT. Stream vectors in Figure 3.3.0c indicate the direction and intensity of the IVT flow.

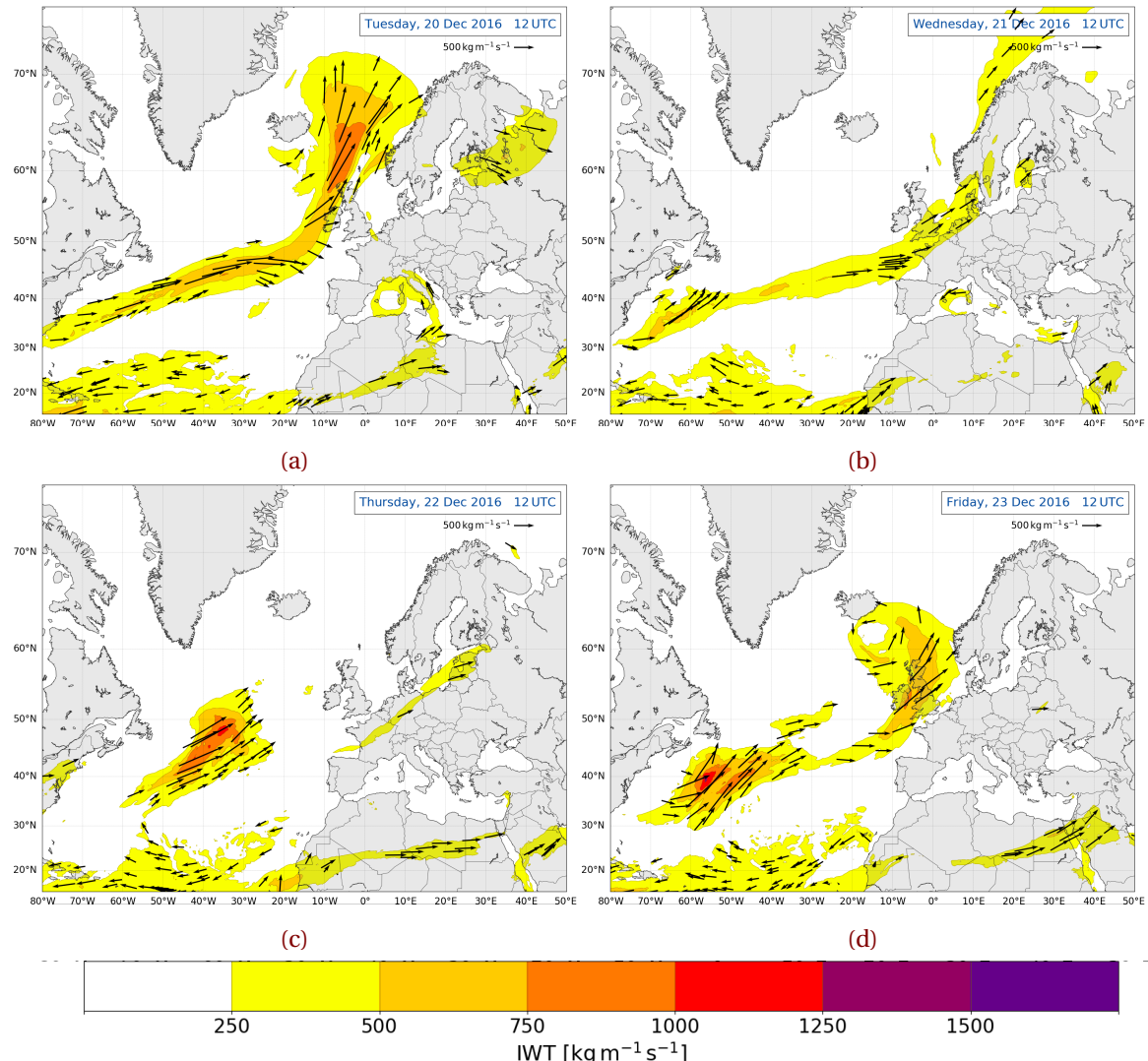


Figure 3.4.1: Atmospheric river analysis map, data from ECMWF. During 20 December 2016 to 27 December 2016. IVT, shaded according to the colour bar [$\text{kg m}^{-1} \text{s}^{-1}$]. Vectors, indicating the direction and magnitude of the IVT.

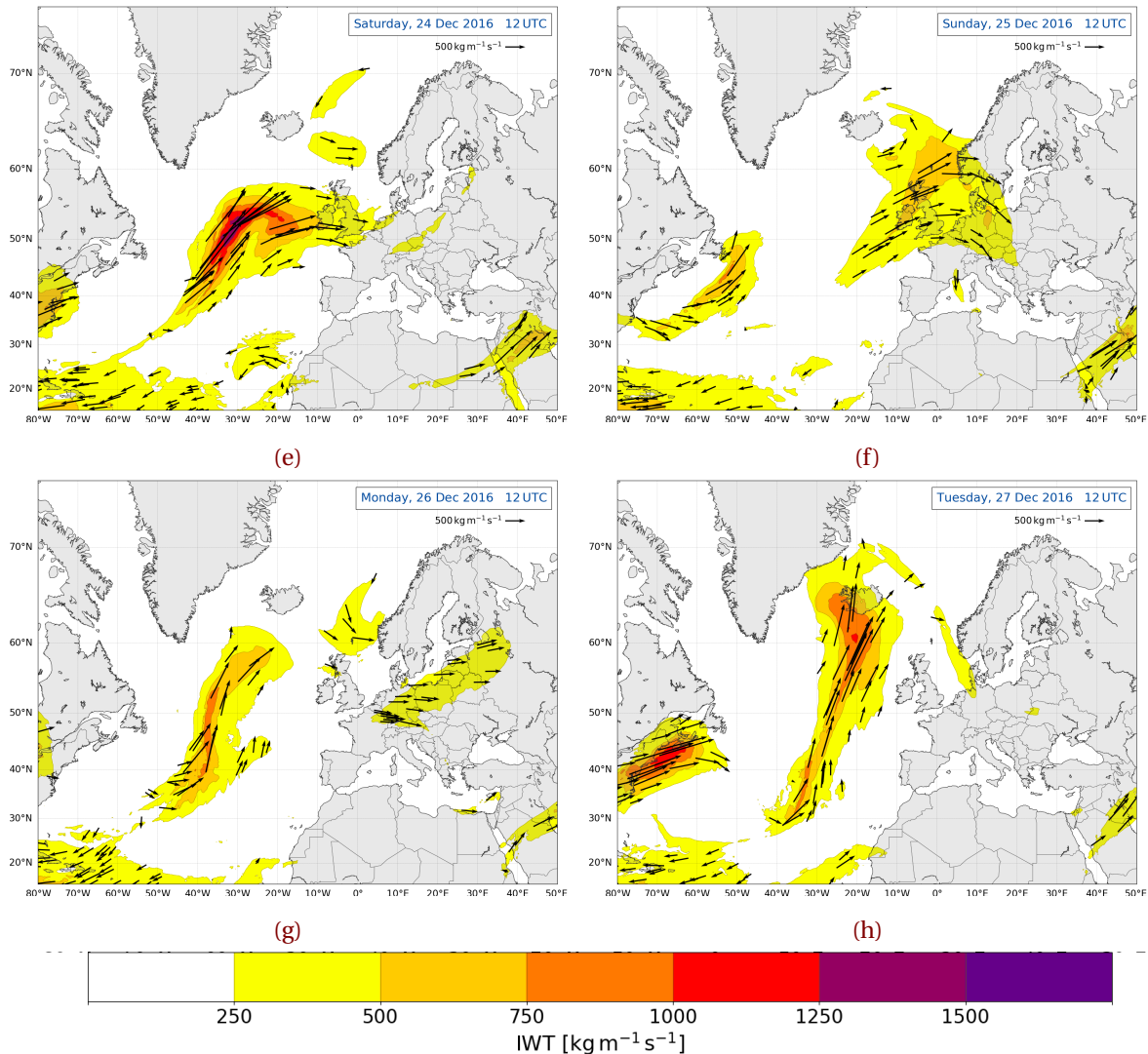


Figure 3.4.1: (Continued from previous page.)

The integrated vapour transport (IVT) was calculated from the ECMWF data as followed:

$$IVT = \frac{1}{g} \int_{p_{sfc}}^{100\text{hPa}} qVdp \quad [\text{kg m}^{-1} \text{s}^{-1}] \quad (3.4.1)$$

where g is the standard gravity, q the specific humidity, and \mathbf{V} the total wind vector at each pressure level p . The numerical, trapezoidal integration is performed by using data from the surface pressure p_{sfc} to 850 hPa in 50 hPa intervals and from 700 hPa to 100 hPa in 100 hPa intervals.

Analysing integrated vapour transport maps is important, since extreme precipitation events in Norway are often influenced by moist, warm air advection from the tropics [Azad and Sorteberg, 2017]. Figure 3.4.1 shows integrated vapour transport from the tropics to the midlatitudes, but it also presents that the occurrence of the atmospheric river was not the main factor which led to intense precipitation during the 2016 Christmas storm. Since it showed not to be intense it will not be further discussed.

3.5 OBSERVATIONS AT THE WEATHER MAST

It is a primary goal of this work to relate the local weather observations from the WMO site at Haukeliseter to the synoptic scale structure and the additional measurements taken at Haukeliseter during the winter of 2016/2017.

Examples of the 60 min precipitation accumulation from the double fence rain gauge, 2 m air temperature, and wind observations are presented in Figure 3.5.1 to document the continuous precipitation at Haukeliseter during the extreme event. The temperature evolution will be used to investigate possible changes in the type of precipitation.

Snowfall is likely for temperatures up to 2 °C. The intensity of the storm can be classified by the hourly averaged wind speed and direction as wind barbs in m s^{-1} . To understand which damage a storm can have, Færaas et al. [2016] released a table to associate wind strength with damage (see Table 3.1.1).

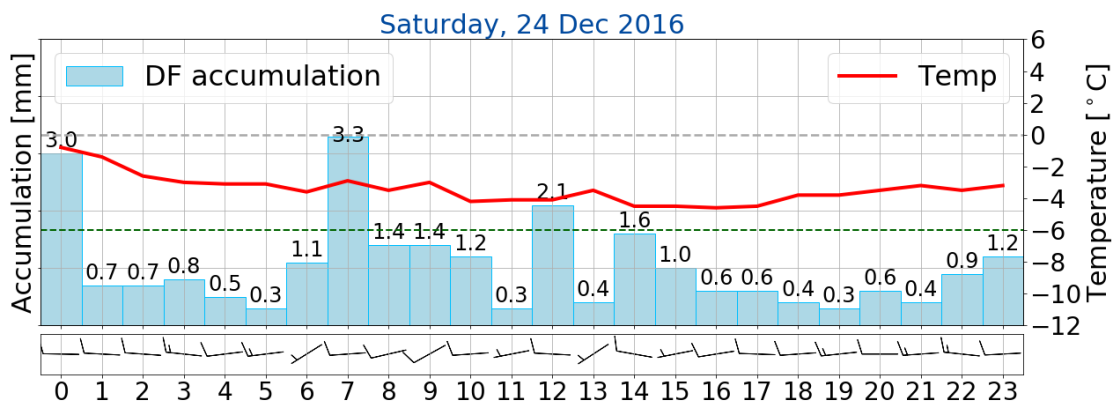


Figure 3.5.1: Surface precipitation, 2m temperature and 10 m wind observation from the weather mast at Haukeliseter on 24 December 2016. 60 min total accumulation [mm] in light blue as bar, temperature (red, [°C]), and 10 min averaged wind as barbs [m s^{-1}]. Gray dashed line indicates the freezing temperature and the green dashed line the 30-year climate mean temperature of -6 °C. Hourly processed data taken from [eklima \[2016\]](#).

3.6 LARGE SCALE CIRCULATION

It has long been known that precipitation and temperature fluctuations occur during European winter in connection with NAO (North Atlantic Oscillation). The NAO is a redistribution of atmospheric mass between the North Atlantic high (Azores high), and the polar low (Iceland low). The NAO index is defined as the gradient between the sea level pressure of the Azores high and the Icelandic low during the winter months (December - March) [Hurrell, 1995]. Positive index shows the deepening of the Icelandic low and a strengthening of the Azores high and negative indexes respectively [Uvo, 2003].

Positive NAO is associated with stronger westerlies than usual across the middle latitudes of the Atlantic [Uvo, 2003]. In addition, more moisture is transported to Scandinavia [Hurrell, 1995]. A positive NAO during winter is often associated with higher temperatures than normal and with an increase in precipitation in northern Europe and low temperatures in southern Europe [Uvo, 2003]. In December 2016, the NAO was positive, with + 0.4, and negative sea level pressure for the Iceland low [Shi et al., 2016], which might explain the incident of the extreme Christmas storm in 2016.

19 TO 20 December 2016

A precursor to extreme storm Urd was a high-pressure system over Scandinavia and an occluded low to the proximate east of Iceland (Figure 3.6.1a, c). Over the coming 36 h a confluence of events resulted in a suppressed tropopause and cold air over Haukeliseter: a filament of a cut off low to the south and cold air advection from the north-east (Figure 3.6.1a, c).

21 December 2016

Associated with the previously mentioned occluded cyclone, cold air impinges on Scandinavia on 21 December 2016 (Figure 3.6.1b, d). Moisture is transported from the low latitudes to high latitudes, influencing Norway's west coast. The westerly flow in Figure 3.6.1d is additionally conducive to orographic lifting. This is coincident with the onset of precipitation at Haukeliseter at 10 UTC on 21 December 2016 (Figure 3.6.1f). Furthermore, given the low temperatures, solid phase precipitation is observed.

Additionally, cyclogenesis is observed off the east coast of the United States (as evidenced by a trough to the northwest of low-level averaged relative vorticity).

22 December 2016

Twenty-four hours later the analysis from 22 December 2016 shows cold air remaining over Scandinavia (Figure 3.6.1g, h). Continues frozen precipitation is observed at Haukeliseter (Figure 3.6.1i). The previously mentioned cyclone is observed to intensify during this time period along the baroclinic zone. The upper-level trough to the north-east of the low-level cyclone centre represents an optimal configuration for cyclone development, since the surface low is located below the temperature gradient at the 2 PVU surface (Figure 3.6.1g, h). This is apparent in the intensification of the surface system (low-level averaged vorticity and mean sea level pressure minima) at 50° N. Also, in

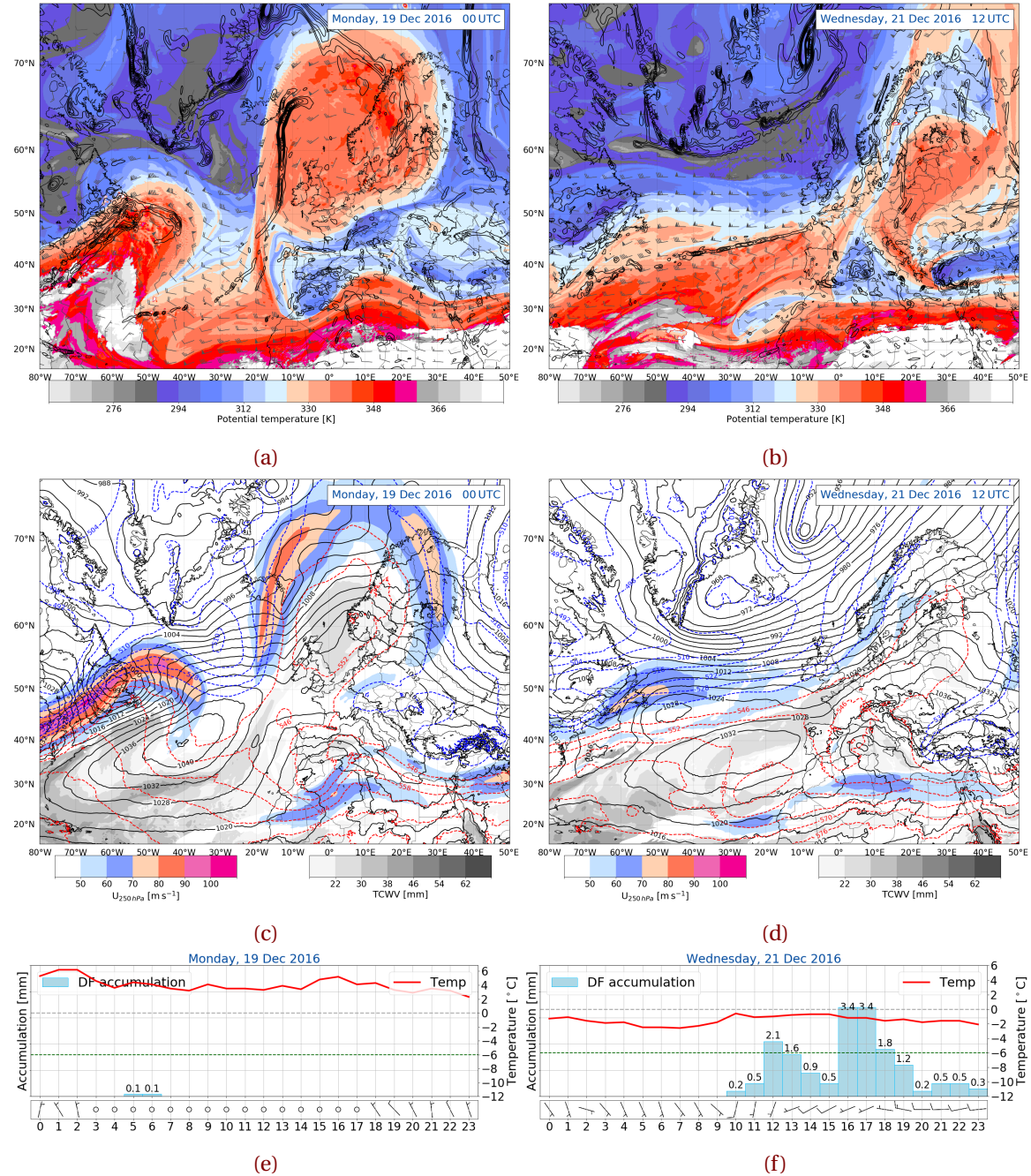


Figure 3.6.1: ECMWF analysis for dynamic tropopause (a, b) as described in Section 3.2, thickness map (c, d) as evaluated in Section 3.3, and local observations at Haukeliseter (e, f; Section 3.5). Analysis is shown for 19 December 2016 at 00 UTC (left column), and 21 December 2016 at 12 UTC (right column). *Continued on next page.*

evidence is the diabatic ridging associated with the ascending warm conveyor belt air-stream (see warm colours in Figure 3.6.1g).

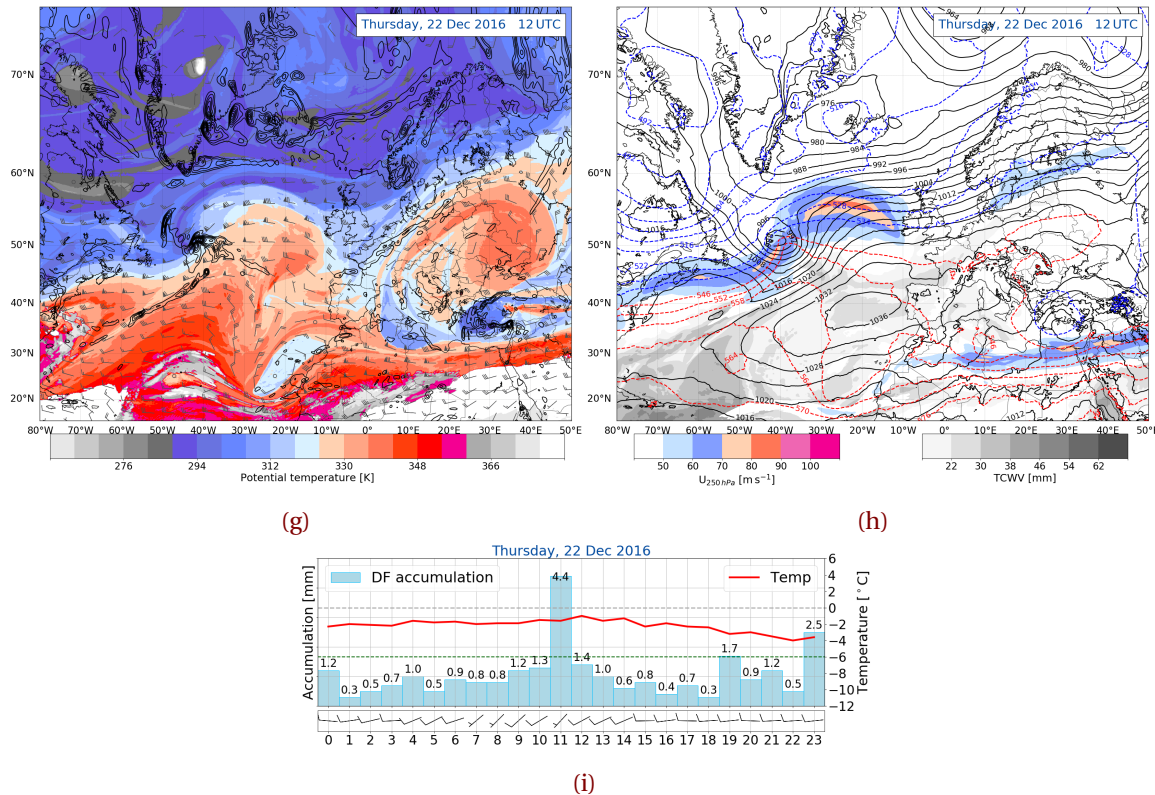


Figure 3.6.1: (Continued from previous page.) 22 December 2016 at 12 UTC.

23 December 2016

The west Atlantic cyclone translates along the jet stream (Figure 3.6.1l, m). The occluded front of the storm arrives roughly between 6 UTC and 12 UTC. By 12 UTC an elevated tropopause is observed in Figure 3.6.1j. The surface temperature rises (Figure 3.6.1n), and mixed phase precipitation is related to the increased temperature and moisture transport from the low latitudes Figure 3.6.1l. A cyclogenesis event occurs in the west Atlantic with a similar disposition of an upper-level trough and a low-level baroclinic zone at 40° N (Figures 3.6.1j to 3.6.1m).

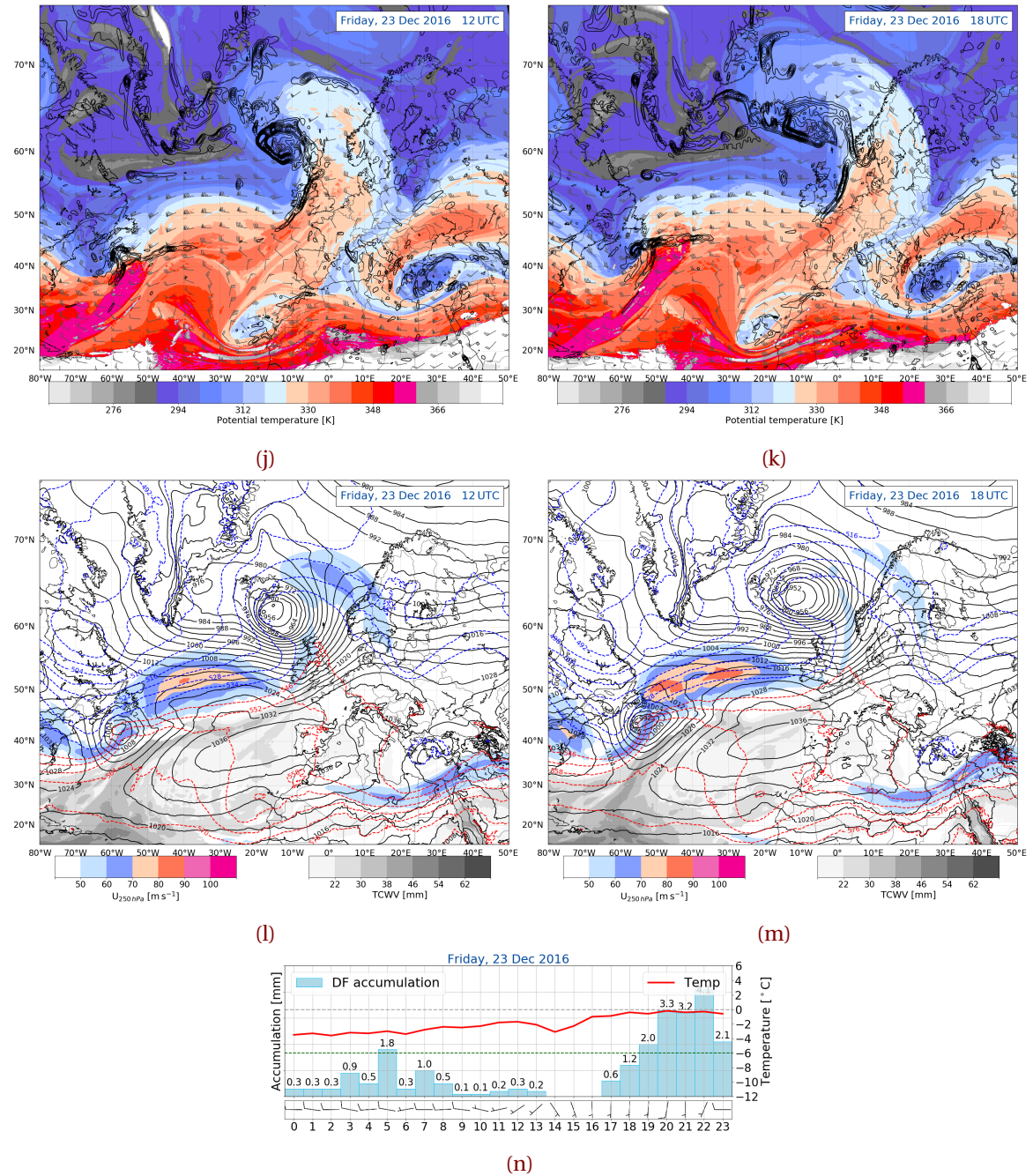


Figure 3.6.1: (Continued from previous page.) For 23 December 2016 at 12 UTC (j, l) and at 18 UTC (k, m).

24 December 2016

After the passage of the occluded front over Norway, passes cold air into Scandinavia (Figure 3.6.1o, p). The temperature drops in Figure 3.6.1q), and solid phase precipitation resumes. The importance of moisture transport is emphasized by the integrated water vapour plot (Figure 3.4.1e). This represents a crucial component to the high precipitation amounts that were measured at the observational site. This represents a quantitative confirmation of previous climatological studies of extreme, cold-season precipitation [Azad and Sorteberg, 2017, Moore, unpublished].

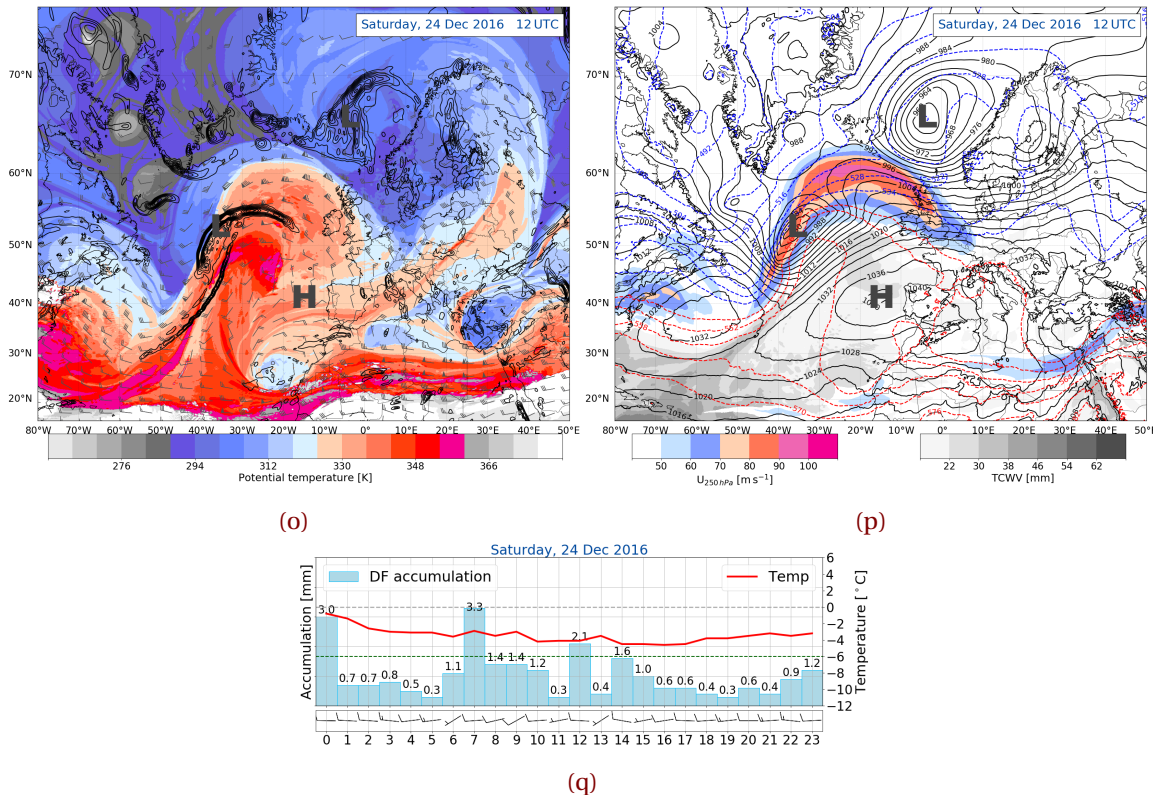


Figure 3.6.1: (Continued from previous page.) 24 December 2016 at 12 UTC.

25 December 2016

Twenty-four hours later the upper level ridge is more pronounced and covers large parts of Norway (Figure 3.6.1r). The cyclone south-east of Iceland has built its frontal boundaries (Figure 3.6.1t). Between 12 UTC and 18 UTC the warm sector passes through Haukeliseter (Figure 3.6.1t, u, v). Connected to the warm sector the temperature rises in Figure 3.6.1v and the precipitation becomes liquid.

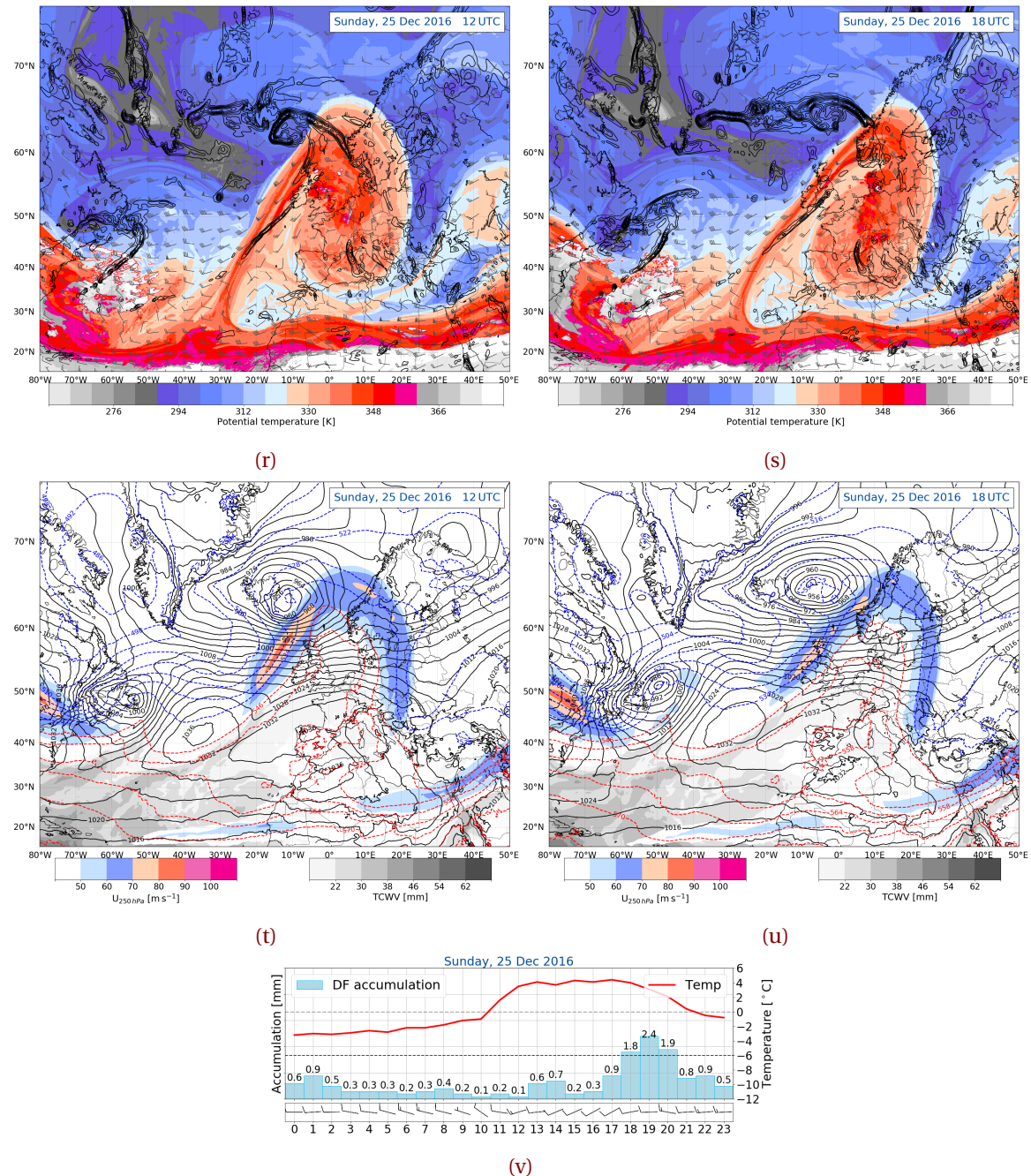


Figure 3.6.1: (Continued from previous page.) For 25 December 2016 at 12 UTC (r, t) and at 18 UTC (s, u).

26 December 2016

Within the next twenty-four hours the cold sector comes through Haukeliseter and Norway is covered in cold air (Figure 3.6.1w, z) cold sector comes through. The surface pressure indicates the occlusion of the cyclone and therefore a weakening and dissipation by 18 UTC. A drop in temperature and a change in precipitation phase is observed at Haukeliseter (Figure 3.6.1aa).

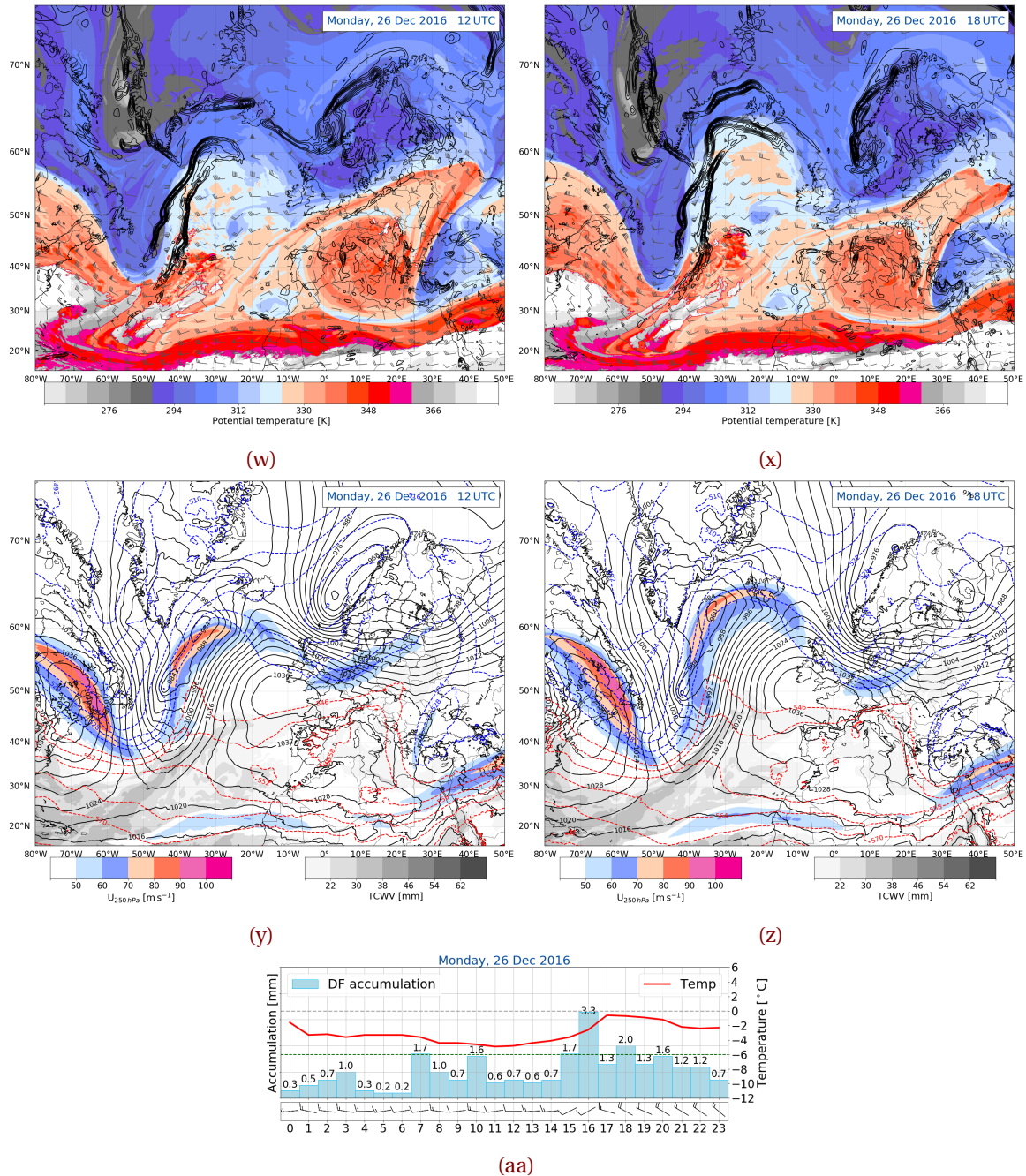


Figure 3.6.1: (Continued from previous page.) For 26 December 2016 at 12 UTC (w, y) and at 18 UTC (x, z).

LIST OF ABBREVIATIONS

ACC	Accretion
AGG	Aggregation
AR	Atmospheric River
AROME	Applications of Research to Operations at Mesoscale
AUT	Autoconversion
BER	Bergeron-Findeisen process
C3VP	Canadian CloudSat-CALIPSO Validation Project
CFR	Contact Freezing of Raindrops
CPR	Cloud Profiling Radar
CV	Coefficient of Variation
CVM	Conversion-melting
DDA	Discrete Dipole Approximation
DEP	Deposition
DRY	Dry processes
DT	Dynamic Tropopause
ECMWF	European Centre for Medium-Range Weather Forecasts
EPS	Ensemble Prediction System
FMI	Finnish Meteorological Institute
HEN	Heterogeneous Nucleation
HON	Homogeneous Nucleation
IVT	Integrated Vapour Transport
LWC	Liquid Water Content

MASC	Multi-Angular Snowfall Camera
MEPS	MetCoOp Ensemble Prediction System
Meso-NH	Mesoscale Non-Hydrostatic model
Met-Norway	Norwegian Meteorological Institute
MetCoOp	Meteorological Co-operation on Operational NWP
MLT	Melting
MRR	Micro Rain Radar
MSLP	Mean Sea Level Pressure
NSF	National Science Foundation
NWP	Numerical Weather Prediction
PIP	Precipitation Imaging Package
PSD	Particle Size distribution
RIM	Riming
SMHI	Swedish Meteorological and Hydrological Institute
SWC	Snow Water Content
SWP	Snow Water Path
WCB	Warm Conveyor Belt
WET	Wet processes
WMO	World Meteorological Organization

REFERENCES

- Azad, R. and Sorteberg, A. Extreme daily precipitation in coastal western Norway and the link to atmospheric rivers. *Journal of Geophysical Research: Atmospheres*, 122(4):2080–2095, January 2017. ISSN 2169-8996. doi: 10.1002/2016JD025615. URL <https://agupubs.onlinelibrary.wiley.com/doi/abs/10.1002/2016JD025615>.
- Barnett, T. P., Adam, J. C., and Lettenmaier, D. P. Potential impacts of a warming climate on water availability in snow-dominated regions. *Nature*, 438(7066):303–309, November 2005. ISSN 1476-4687. doi: 10.1038/nature04141. URL <https://www.nature.com/articles/nature04141>.
- Buizza, R., Hollingsworth, A., Lalaurette, F., and Ghelli, A. Probabilistic Predictions of Precipitation Using the ECMWF Ensemble Prediction System. *Wea. Forecasting*, 14(2):168–189, April 1999. ISSN 0882-8156. doi: 10.1175/1520-0434(1999)014<0168:PPOPUT>2.0.CO;2. URL <https://journals.ametsoc.org/doi/full/10.1175/1520-0434%281999%29014%3C0168%3APP0PUT%3E2.0.CO%3B2>.
- Caniaux, G., Redelsperger, J.-L., and Lafore, J.-P. A Numerical Study of the Stratiform Region of a Fast-Moving Squall Line. Part I: General Description and Water and Heat Budgets. *J. Atmos. Sci.*, 51(14):2046–2074, July 1994. ISSN 0022-4928. doi: 10.1175/1520-0469(1994)051<2046:ANSOTS>2.0.CO;2. URL [https://journals.ametsoc.org/doi/abs/10.1175/1520-0469\(1994\)051%3C2046:ANSOTS%3E2.0.CO;2](https://journals.ametsoc.org/doi/abs/10.1175/1520-0469(1994)051%3C2046:ANSOTS%3E2.0.CO;2).
- Christensen, M. W., Behrangi, A., L'ecuyer, T. S., Wood, N. B., Lebsack, M. D., and Stephens, G. L. Arctic Observation and Reanalysis Integrated System: A New Data Product for Validation and Climate Study. *Bull. Amer. Meteor. Soc.*, 97(6):907–916, January 2016. ISSN 0003-0007. doi: 10.1175/BAMS-D-14-00273.1. URL <https://journals.ametsoc.org/doi/10.1175/BAMS-D-14-00273.1>.
- Cooper, S. J., Wood, N. B., and L'Ecuyer, T. S. A variational technique to estimate snowfall rate from coincident radar, snowflake, and fall-speed observations. *Atmos. Meas. Tech.*, 10(7):2557–2571, July 2017. ISSN 1867-8548. doi: 10.5194/amt-10-2557-2017. URL <https://www.atmos-meas-tech.net/10/2557/2017/>.
- Dahlgren, P. A Comparison Of Two Large Scale Blending Methods. page 16, 2013. URL <http://metcoop.org/memo/2013/02-2013-METCOOP-MEMO.PDF>.
- Dando, P. Introducing the octahedral reduced Gaussian grid, June 2016. URL <https://software.ecmwf.int/wiki/display/FCST/Gaussian+grids>.
- Doviak, R. J. and Zrnic, D. S. *Doppler Radar and Weather Observations*. Courier Corporation, 1993. ISBN 978-0-486-45060-5. Google-Books-ID: ispLkPX9n2UC.

- eklma. Norwegian Meteorological Institute, 2016. URL http://sharki.oslo.dnmi.no/portal/page?_pageid=73,39035,73_39049&_dad=portal&_schema=PORTAL.
- Færaas, A., Rommetveit, A., Duesund, J., and Senel, E. «Urd» har nådd orkan styrke – flytter seg mot Østlandet, December 2016. URL http://www.yr.no/artikkelen/_urd_-har-nadd-orkan-styrke--flytter-seg-mot-ostlandet-1.13292245.
- Farestveit, E. 80.000 mista radioen under ekstremvêret, December 2016. URL <https://www.nrk.no/hordaland/80.000-mista-radioen-under-ekstremveret-1.13294980>.
- Field, C. B., Barros, V. R., Dokken, D. J., Mach, K. J., Mastrandrea, M. D., Bilir, T. E., Chatterjee, M., Ebi, K. L., Estrada, Y. O., Genova, R. C., Girma, B., Kissel, E. S., Levy, A. N., MacCracken, S., Mastrandrea, P. R., and White, L. L. Summary for policymakers. In: Climate Change 2014: Impacts, Adaptation, and Vulnerability. Part A: Global and Sectoral Aspects. Contribution of Working Group II to the Fifth Assessment Report of the Intergovernmental Panel on Climate Change. Cambridge: Cambridge University Press, page 34, 2014.
- Garrett, T. J., Fallgatter, C., Shkurko, K., and Howlett, D. Fall speed measurement and high-resolution multi-angle photography of hydrometeors in free fall. *Atmos. Meas. Tech.*, 5(11):2625–2633, November 2012. ISSN 1867-8548. doi: 10.5194/amt-5-2625-2012. URL <https://www.atmos-meas-tech.net/5/2625/2012/>.
- Geonor Inc. T-200b All Weather Precipitation – Rain Gauge, 2015. URL <http://geonor.com/live/products/weather-instruments/t-200b-weather-precipitation-rain-gauge/>.
- Geonorge. DTM 10 Terrengmodell (UTM33) - Kartverket - Kartkatalogen, May 2018. URL <https://kartkatalog.geonorge.no/metadata/uuid/dddbb667-1303-4ac5-8640-7ec04c0e3918>.
- Goodison, B. E., Louie, P. Y. T., and Yang, D. WMO Solid Precipitation Measurement Intercomparison: Final Report. Instruments and Observing Methods Rep. 67, WMO/TD-No. 872,. World Meteorological Organization, Geneva, Switzerland, page 318, 1998.
- Gowan, T. M., Steenburgh, W. J., and Schwartz, C. S. Validation of Mountain Precipitation Forecasts from the Convection-Permitting NCAR Ensemble and Operational Forecast Systems over the Western United States. *Wea. Forecasting*, 33(3):739–765, June 2018. ISSN 0882-8156, 1520-0434. doi: 10.1175/WAF-D-17-0144.1. URL <http://journals.ametsoc.org/doi/10.1175/WAF-D-17-0144.1>.
- Hansen, B. B., Isaksen, K., Benestad, R. E., Kohler, J., Pedersen, Ø. Ø., Loe, L. E., Coulson, S. J., Larsen, J. O., and Varpe, Ø. Warmer and wetter winters: characteristics and implications of an extreme weather event in the High Arctic. *Environ. Res. Lett.*, 9(11):114021, 2014. ISSN 1748-9326. doi: 10.1088/1748-9326/9/11/114021. URL <http://stacks.iop.org/1748-9326/9/i=11/a=114021>.
- Homleid, M. and Tveter, F. T. Verification of operational weather prediction models september to november 2015. *METInfo Rep.*, 16:2016, 2016. URL https://www.met.no/publikasjoner/met-info/met-info-2016/_attachment/download/b0463915-cba0-42ac-8539-4233ae2bf01c:3d71565a27f88085373199a33ab8569151c144e9/MET-info-22-2016.pdf.
- Hudak, D., Barker, H., Rodriguez, P., and Donovan, D. The Canadian CloudSat Validation Project.

- 4th ERAD, September 2006. URL <http://www.crahi.upc.edu/ERAD2006/proceedingsMask/00165.pdf>. Barcelona, Spain.
- Hurrell, J. W. Decadal Trends in the North Atlantic Oscillation: Regional Temperatures and Precipitation. *Science*, 269(5224):676–679, August 1995. ISSN 0036-8075, 1095-9203. doi: [10.1126/science.269.5224.676](https://doi.org/10.1126/science.269.5224.676). URL <http://science.sciencemag.org/content/269/5224/676>.
- Joos, H. and Wernli, H. Influence of microphysical processes on the potential vorticity development in a warm conveyor belt: a case-study with the limited-area model COSMO. *Q. J. Royal Meteorol. Soc.*, 138(663):407–418, January 2012. ISSN 00359009. doi: [10.1002/qj.934](https://doi.org/10.1002/qj.934). URL <http://doi.wiley.com/10.1002/qj.934>.
- Kalnay, E. *Atmospheric modeling, data assimilation and predictability*. Cambridge University Press, Cambridge, 2003. ISBN 978-0-521-79179-3.
- Kartverket. Norgeskart, November 2018. URL http://www.norgeskart.no/?_ga=2.7509489.291164698.1524482471-1352211079.1517515119#!?project=seeiendom&layers=1002,1015&zoom=4&lat=7197864.00&lon=396722.00.
- Kochendorfer, J., Nitu, R., Wolff, M., Mekis, E., Rasmussen, R., Baker, B., Earle, M. E., Reverdin, A., Wong, K., Smith, C. D., Yang, D., Roulet, Y.-A., Buisan, S., Laine, T., Lee, G., Aceituno, J. L. C., Alastraú, J., Isaksen, K., Meyers, T., Brækkan, R., Landolt, S., Jachcik, A., and Poikonen, A. Analysis of single-Alter-shielded and unshielded measurements of mixed and solid precipitation from WMO-SPICE. *Hydrol. Earth Syst. Sci.*, 21(7):3525–3542, July 2017. ISSN 1607-7938. doi: [10.5194/hess-21-3525-2017](https://doi.org/10.5194/hess-21-3525-2017). URL <https://www.hydrol-earth-syst-sci.net/21/3525/2017/>.
- Køltzow, M. A. Ø. Spin-up time of MEPS. Private Communication, 2018.
- Kulie, M. S. and Bennartz, R. Utilizing Spaceborne Radars to Retrieve Dry Snowfall. *J. Appl. Meteor. Climatol.*, 48(12):2564–2580, January 2009. ISSN 1558-8424. doi: [10.1175/2009JAMC2193.1](https://doi.org/10.1175/2009JAMC2193.1). URL <http://journals.ametsoc.org/doi/abs/10.1175/2009JAMC2193.1>.
- Kulie, M. S., Milani, L., Wood, N. B., Tushaus, S. A., Bennartz, R., and L'Ecuyer, T. S. A Shallow Cumuliform Snowfall Census Using Spaceborne Radar. *J. Hydrometeor.*, 17(4):1261–1279, February 2016. ISSN 1525-755X. doi: [10.1175/JHM-D-15-0123.1](https://doi.org/10.1175/JHM-D-15-0123.1). URL <https://journals.ametsoc.org/doi/abs/10.1175/JHM-D-15-0123.1>.
- Køltzow, M. A. MetCoOp EPS - A convection permitting ensemble prediction system, October 2017.
- L'Ecuyer, T. S. AOS 441 - Satellite and Radar Meteorology. January 2017. URL <https://lecuyer.aos.wisc.edu/aos441>.
- Liu G. Deriving snow cloud characteristics from CloudSat observations. *J. Geophys. Res. Atmos.*, 113(D8), September 2008. ISSN 0148-0227. doi: [10.1029/2007JD009766](https://doi.org/10.1029/2007JD009766). URL <https://agupubs.onlinelibrary.wiley.com/doi/abs/10.1029/2007JD009766>.
- Lorenz, E. N. Atmospheric Predictability as Revealed by Naturally Occurring Analogues. *J. Atmos. Sci.*, 26(4):636–646, July 1969. ISSN 0022-4928. doi: [10.1175/1520-](https://doi.org/10.1175/1520-)

- 0469(1969)26<636:APARBN>2.0.CO;2. URL <https://journals.ametsoc.org/doi/abs/10.1175/1520-0469%281969%2926%3C636%3AAPARBN%3E2.0.CO%3B2>.
- Markowski, P. and Richardson, Y. *Mesoscale Meteorology in Midlatitudes*. John Wiley & Sons, September 2011. ISBN 978-1-119-96667-8. Google-Books-ID: MDeYosfLLEYC.
- Martin, J. E. *Mid-Latitude Atmospheric Dynamics: A First Course*. Wiley, May 2006. ISBN 978-0-470-86466-1.
- McCumber, M., Tao, W.-K., Simpson, J., Penc, R., and Soong, S.-T. Comparison of Ice-Phase Microphysical Parameterization Schemes Using Numerical Simulations of Tropical Convection. *J. Appl. Meteor.*, 30(7):985–1004, July 1991. ISSN 0894-8763. doi: [10.1175/1520-0450-30.7.985](https://doi.org/10.1175/1520-0450-30.7.985). URL <https://journals.ametsoc.org/doi/abs/10.1175/1520-0450-30.7.985>.
- Meehl, G. A., Karl, T., Easterling, D. R., Changnon, S., Pielke, R., Changnon, D., Evans, J., Groisman, P. Y., Knutson, T. R., Kunkel, K. E., Mearns, L. O., Parmesan, C., Pulwarty, R., Root, T., Sylves, R. T., Whetton, P., and Zwiers, F. An Introduction to Trends in Extreme Weather and Climate Events: Observations, Socioeconomic Impacts, Terrestrial Ecological Impacts, and Model Projections. *Bull. Amer. Meteor. Soc.*, 81(3):413–416, March 2000. ISSN 0003-0007. doi: [10.1175/1520-0477\(2000\)081<0413:AITTIE>2.3.CO;2](https://doi.org/10.1175/1520-0477(2000)081<0413:AITTIE>2.3.CO;2). URL [https://journals.ametsoc.org/doi/abs/10.1175/1520-0477\(2000\)081%3C0413:AITTIE%3E2.3.CO;2](https://journals.ametsoc.org/doi/abs/10.1175/1520-0477(2000)081%3C0413:AITTIE%3E2.3.CO;2).
- MetCoOp Wiki. Description of MEPS, December 2017. URL <https://metcoop.smhi.se/dokuwiki/nwp/metcoop/>.
- METEK, M. M. G. Micro Rain Radar MRR-2, October 2010. URL <http://metek.de/wp-content/uploads/2014/05/Metek-Micro-Rain-Radar-MRR-2-Datasheet.pdf>.
- Meteo France. The Meso-NH Atmospheric Simulation System: Scientific Documentation, Part III: Physics, January 2009.
- Meteorologene. "Her kommer #Urd! Selve Lavtrykksenteret treffer Møre og Romsdal, men den sterkeste vinden kommer sør for Stad. #SørNorge" 26 December 2016, 9:34am, 2016. URL <https://twitter.com/Meteorologene>.
- Moore, R. Large-scale dynamics inducing atmospheric rivers and extreme precipitation over norway. unpublished.
- Müller, M., Homleid, M., Ivarsson, K.-I., Køltzow, M. A. Ø., Lindskog, M., Midtbø, K. H., Andrae, U., Aspelien, T., Berggren, L., Bjørge, D., Dahlgren, P., Kristiansen, J., Randriamampianina, R., Ridal, M., and Vignes, O. AROME-MetCoOp: A Nordic Convective-Scale Operational Weather Prediction Model. *Wea. Forecasting*, 32(2):609–627, January 2017. ISSN 0882-8156. doi: [10.1175/WAF-D-16-0099.1](https://doi.org/10.1175/WAF-D-16-0099.1). URL <https://journals.ametsoc.org/doi/abs/10.1175/WAF-D-16-0099.1>.
- Newman, A. J., Kucera, P. A., and Bliven, L. F. Presenting the Snowflake Video Imager (SVI). *J. Atmos. Oceanic Technol.*, 26(2):167–179, February 2009. ISSN 0739-0572. doi: [10.1175/2008JTECH1148.1](https://doi.org/10.1175/2008JTECH1148.1). URL <https://journals.ametsoc.org/doi/abs/10.1175/2008JTECH1148.1>.
- Nielsen-Gammon, J. W. A Visualization of the Global Dynamic Tropopause. *Bull. Amer. Meteor. Soc.*, 82(6):1151–1168, June 2001. ISSN 0003-0007. doi: [10.1175/1520-0469%282001%2982%3A%3D%3E2.0.CO%3B2](https://doi.org/10.1175/1520-0469%282001%2982%3A%3D%3E2.0.CO%3B2).

- 0477(2001)082<1151:AVOTGD>2.3.CO;2. URL [https://journals.ametsoc.org/doi/abs/10.1175/1520-0477\(2001\)082%3C1151:AVOTGD%3E2.3.CO;2](https://journals.ametsoc.org/doi/abs/10.1175/1520-0477(2001)082%3C1151:AVOTGD%3E2.3.CO;2).
- Noh, Y.-J., Liu, G., Seo, E.-K., Wang, J. R., and Aonashi, K. Development of a snowfall retrieval algorithm at high microwave frequencies. *J. Geophys. Res.*, 111(D22), November 2006. ISSN 2156-2202. doi: 10.1029/2005JD006826. URL <https://agupubs.onlinelibrary.wiley.com/doi/abs/10.1029/2005JD006826>.
- Norin, L., Devasthale, A., L'Ecuyer, T. S., Wood, N. B., and Smalley, M. Intercomparison of snowfall estimates derived from the CloudSat Cloud Profiling Radar and the ground-based weather radar network over Sweden. *Atmos. Meas. Tech.*, 8(12):5009–5021, December 2015. ISSN 1867-8548. doi: 10.5194/amt-8-5009-2015. URL <https://www.atmos-meas-tech.net/8/5009/2015/>.
- Norwegian Meteorological Institute. MET Norway Thredds Service, 2016. URL <http://thredds.met.no/thredds/catalog/meps25epsarchive/catalog.html>.
- Olsen, A.-M. and Granerød, M. Ekstremværrapport. Hendelse: Urd 26. desember met. info. no. 18/2017 ISSN X METEOROLOGI Bergen, - PDF, September 2017. URL <http://docplayer.me/48734203-Ekstremvaerrapport-hendelse-urd-26-desember-met-info-no-18-2017-issn-x-meteorologi-bergen.html>.
- Palerme, C., Kay, J. E., Genthon, C., L'Ecuyer, T., Wood, N. B., and Claud, C. How much snow falls on the Antarctic ice sheet? *The Cryosphere*, 8(4):1577–1587, August 2014. ISSN 1994-0424. doi: 10.5194/tc-8-1577-2014. URL <https://www.the-cryosphere.net/8/1577/2014/>.
- Palerme, C., Genthon, C., Claud, C., Kay, J. E., Wood, N. B., and L'Ecuyer, T. Evaluation of current and projected Antarctic precipitation in CMIP5 models. *Clim. Dyn.*, 48(1-2):225–239, January 2017. ISSN 0930-7575, 1432-0894. doi: 10.1007/s00382-016-3071-1. URL <https://link.springer.com/article/10.1007/s00382-016-3071-1>.
- Pedersen, K. and Rommetveit, A. Hva er et «ekstremvær»?, November 2013. URL http://www.yr.no/artikkel/hva-er-et-_ekstremvaer__-1.7890946.
- Peel, M. C., Finlayson, B. L., and McMahon, T. A. Updated world map of the Köppen-Geiger climate classification. *Hydrology and Earth System Sciences Discussions*, 4(2):439–473, March 2007. URL <https://hal.archives-ouvertes.fr/hal-00298818>.
- Petroliagis, T., Buizza, R., Lanzinger, A., and Palmer, T. N. Potential use of the ECMWF Ensemble Prediction System in cases of extreme weather events. *Meteorological Applications*, 4(1):69–84, March 1997. ISSN 1469-8080, 1350-4827. URL <https://www.cambridge.org/core/journals/meteorological-applications/article/potential-use-of-the-ecmwf-ensemble-prediction-system-in-cases-of-extreme-weather-events/C63050704CB35CD43BC4E5998A390DDC>.
- Pinty, J.-P. and Jabouille, P. A mixed-phased cloud parameterization for use in a mesoscale non-hydrostatic model: Simulations of a squall line and of orographic precipitation. pages 217–220. Amer. Meteor. Soc., 1998.
- Rinehart, R. E. *Radar for Meteorologists: Or You, Too, Can be a Radar Meteorologist*. Rinehart Publications, 2010. ISBN 978-0-9658002-3-5. Google-Books-ID: VqatcQAACAAJ.

- Rutz, J. J., Steenburgh, W. J., and Ralph, F. M. Climatological Characteristics of Atmospheric Rivers and Their Inland Penetration over the Western United States. *Mon. Wea. Rev.*, 142(2):905–921, January 2014. ISSN 0027-0644. doi: 10.1175/MWR-D-13-00168.1. URL <http://journals.ametsoc.org/doi/abs/10.1175/MWR-D-13-00168.1>.
- Ruud, S., Carr Ekroll, H., Bakke Foss, A., Torgersen, H. O., and Annar Holm, P. To tonn tungt skilt blåste ned da ekstremværet traff Oslo og Østlandet i natt, December 2016. URL <https://www.aftenposten.no/article/ap-2z6wy.html>.
- Schirle, C. Characterization of snowfall at high latitudes using an optimal estimation-based retrieval algorithm. Private Communication, 2018.
- Shi, W., L'Heureux, M., and Halpert, M. Climate Diagnostics Bulletin - December 2016, Near Real-Time Ocean/Atmosphere: Monitoring, Assessments, and Prediction. Technical report, Climate Prediction Center, 2016. URL http://origin.cpc.ncep.noaa.gov/products/CDB/CDB_Archive_pdf/PDF/CDB.dec2016_color.pdf.
- Skofronick-Jackson, G. M., Kim, M.-J., Weinman, J. A., and Chang, D.-E. A physical model to determine snowfall over land by microwave radiometry. *IEEE Geosci. Remote Sens. Lett.*, 42(5): 1047–1058, May 2004. ISSN 0196-2892. doi: 10.1109/TGRS.2004.825585.
- Stephens, G. L. *Remote Sensing of the Lower Atmosphere: An Introduction*. Oxford University Press, 1994. ISBN 978-0-19-508188-6. Google-Books-ID: 2FcRAQAAIAAJ.
- Stocker, T. F., Qin, D., Plattner, G.-K., Tignor, M. M. B., Allen, S. K., Boschung, J., Nauels, A., Xia, Y., Bex, V., and Midgley, P. M. Working Group I Contribution to the Fifth Assessment Report of the Intergovernmental Panel on Climate Change. *Cambridge: Cambridge University Press*, page 14, 2013.
- Sun, J. Convective-scale assimilation of radar data: progress and challenges. *Quarterly Journal of the Royal Meteorological Society*, 131(613):3439–3463, 2005. ISSN 1477-870X. doi: 10.1256/qj.05.149. URL <https://rmets.onlinelibrary.wiley.com/doi/abs/10.1256/qj.05.149>.
- Uvo, C. B. Analysis and regionalization of northern European winter precipitation based on its relationship with the North Atlantic oscillation. *International Journal of Climatology*, 23(10):1185–1194, July 2003. ISSN 1097-0088. doi: 10.1002/joc.930. URL <https://rmets.onlinelibrary.wiley.com/doi/abs/10.1002/joc.930>.
- Warner, T. T., Peterson, R. A., and Treadon, R. E. A Tutorial on Lateral Boundary Conditions as a Basic and Potentially Serious Limitation to Regional Numerical Weather Prediction. *Bull. Amer. Meteor. Soc.*, 78(11):2599–2618, November 1997. ISSN 0003-0007. doi: 10.1175/1520-0477(1997)078<2599:ATOLBC>2.0.CO;2. URL [https://journals.ametsoc.org/doi/abs/10.1175/1520-0477\(1997\)078%3C2599:ATOLBC%3E2.0.CO%3B2](https://journals.ametsoc.org/doi/abs/10.1175/1520-0477(1997)078%3C2599:ATOLBC%3E2.0.CO%3B2).
- Wolff, M. A. WMO Solid Precipitation Intercomparison Experiment (WMO-SPICE), Ch. 4.2.4 Precipitation measurements in areas with high winds and/or complex terrain. unpublished.
- Wolff, M. A., Brækkan, R., Isaksen, K., and Ruud, E. A new testsite for wind correction of precipitation measurements at a mountain plateau in southern Norway. In *Proceedings of WMO Technical Conference on Meteorological and Environmental Instruments and Methods of Observation (TECO-2010). Instruments and Observing Methods Report*, 2010.

- Wolff, M. A., Isaksen, K., Brækkan, R., Alfnæs, E., Petersen-Øverleir, A., and Ruud, E. Measurements of wind-induced loss of solid precipitation: description of a Norwegian field study. *Hydrol. Res.*, 44(1):35–43, February 2013. ISSN 0029-1277, 2224-7955. doi: 10.2166/nh.2012.166. URL <http://hr.iwaponline.com/content/44/1/35>.
- Wolff, M. A., Isaksen, K., Petersen-Øverleir, A., Ødemark, K., Reitan, T., and Brækkan, R. Derivation of a new continuous adjustment function for correcting wind-induced loss of solid precipitation: results of a Norwegian field study. *Hydrol. Earth Syst. Sci.*, 19(2):951–967, February 2015. ISSN 1607-7938. doi: 10.5194/hess-19-951-2015. URL <https://www.hydrol-earth-syst-sci.net/19/951/2015/>.
- Wood, N. B. *Estimation of snow microphysical properties with application to millimeter-wavelength radar retrievals for snowfall rate.* Ph.D., Colorado State University, 2011. URL https://dspace.library.colostate.edu/bitstream/handle/10217/48170/Wood_colostate_0053A_10476.pdf?sequence=1&isAllowed=y.
- Wood, N. B., L'Ecuyer, T. S., Vane, D. G., Stephens, G. L., and Partain, P. Level 2c snow profile process description and interface control document. Technical Report, 2013. URL http://www.cloudsat.cira.colostate.edu/sites/default/files/products/files/2C-SNOW-PROFILE_PDICD.P_R04.20130210.pdf.
- Wood, N. B., L'Ecuyer, T. S., Heymsfield, A. J., and Stephens, G. L. Microphysical Constraints on Millimeter-Wavelength Scattering Properties of Snow Particles. *J. Appl. Meteor. Climatol.*, 54(4):909–931, January 2015. ISSN 1558-8424. doi: 10.1175/JAMC-D-14-0137.1. URL <http://journals.ametsoc.org/doi/10.1175/JAMC-D-14-0137.1>.

